

Solomon, *Nature* **355**, 815 (1992).

8. Methane was stripped from seawater in a cooled charcoal trap, and its concentration was determined on a gas chromatograph with a flame ionization detector (reproducibility = 5%). Manganese concentration was measured with a chemiluminescence technique (reproducibility better than 1%) [E. Nakayama, K. Isshiki, Y. Sohrin, H. Karatani, *Anal. Chem.* **61**, 1392 (1989)]. Particulate elemental chemistry was determined by thin-film x-ray fluorescence [R. A. Feely, G. J. Massoth, G. T. Lebon, in *Marine Particles: Analysis and Characterization*, D. C. Hurd and D. W. Spencer, Eds. (Geophysical Monograph 63, American Geophysical Union, Washington, DC, 1991), pp. 251–257]. Helium isotope measurements were made on a 21-cm-radius, dual-collector, statically operated mass spectrometer, with a precision of 0.25% (1 σ) in $\delta(^3\text{He})\%$, the percentage deviation of the $^3\text{He}/^4\text{He}$ ratio from the ratio in air. Microbial cells were filtered onto glass fiber filters with a pore size of 0.2 μ , and fixed in glutaraldehyde.
9. K. C. Macdonald, D. S. Scheirer, S. M. Carbotte, *Science* **253**, 986 (1991).
10. J. M. Sinton, S. M. Smajlik, J. J. Mahoney, K. C. Macdonald, *J. Geophys. Res.* **96**, 6133 (1991).
11. D. S. Scheirer and K. C. Macdonald, *ibid.* **98**, 7871 (1993).
12. E. T. Baker and T. Urabe, in preparation.
13. E. T. Baker, C. R. German, H. Elderfield, in *Physical, Chemical, Biological, and Geological Interactions Within Hydrothermal Systems*, S. Humphris, L. Mullineaux, R. Zierenberg, R. Thomson, Eds. (Geophysical Monograph, American Geophysical Union, Washington, DC, in press).
14. J.-M. Auzende *et al.*, *C. R. Acad. Sci. Paris* **319**, series II, 811 (1994); J.-M. Auzende *et al.*, *Eos* **75**, 601 (1994).
15. K. Fujioka and T. Urabe, unpublished material.
16. J. C. Mutter *et al.*, *Science* **268**, 391 (1995).
17. J. E. Lupton *et al.*, *Geophys. Res. Lett.* **20**, 2913 (1993).
18. R. M. Haymon *et al.*, *Earth Planet. Sci. Lett.* **119**, 85 (1993).
19. E. T. Baker *et al.*, *ibid.* **128**, 1 (1994).
20. R. A. Feely, J. F. Gendron, E. T. Baker, G. T. Lebon, *ibid.*, p. 19.
21. M. J. Mottl *et al.*, *Geochim. Cosmochim. Acta*, in press.

22. D. M. Karl, C. O. Wirsen, H. W. Jannasch, *Science* **207**, 1345 (1980); A. Maruyama *et al.*, *J. Oceanogr.* **49**, 353 (1993).
23. The enrichment of S in hydrothermal plume particles results from precipitation of S-bearing phases from vent fluids strongly enriched in volatile H₂S.
24. E. T. Baker and J. E. Lupton, *Nature* **346**, 556 (1990).
25. K. L. Von Damm *et al.*, *ibid.* **375**, 47 (1995).
26. D. A. Butterfield and G. J. Massoth, *J. Geophys. Res.* **99**, 4951 (1994).
27. G. J. Massoth *et al.*, *ibid.*, p. 4905; T. Gamo *et al.*, *Deep-Sea Res.* **40**, 2335 (1993); C. R. German *et al.*, *Earth Planet. Sci. Lett.* **121**, 647 (1994).
28. R. S. Detrick *et al.*, *Nature* **326**, 35 (1987).
29. J. Phipps Morgan and Y. J. Chen, *ibid.* **364**, 706 (1993).
30. Funded by the Ridge Flux Project of the Science and Technology Agency of Japan and by the VENTS Program of the National Oceanic and Atmospheric Administration.

27 March 1995; accepted 19 June 1995

Catalysis of the Olivine to Spinel Transformation by High Clinoenstatite

T. G. Sharp* and D. C. Rubie

Although enstatite is a major constituent of the Earth's upper mantle and subducting lithosphere, most kinetic studies of olivine phase transformations have typically involved single-phase polycrystalline aggregates. Transmission electron microscopy investigations of olivine to spinel and modified spinel (β phase) reactions in the $(\text{Mg,Fe})_2\text{SiO}_4$ - $(\text{Mg,Fe})\text{SiO}_3$ system show that transformation of olivine in the stability field of spinel plus β phase begins with coherent nucleation of spinel on high-clinoenstatite grains. These observations demonstrate that high clinoenstatite can catalyze the transformation by enhancing nucleation kinetics and therefore imply that secondary phases can influence reaction kinetics during high-pressure mineral transformations.

Seismic discontinuities in the Earth's mantle are generally believed to be caused by high-pressure phase transformations, with a possible additional contribution from compositional stratification (1–3). The 410-km and 660-km discontinuities, for example, define the Earth's transition zone and are correlated with, respectively, the transformation of $(\text{Mg,Fe})_2\text{SiO}_4$ olivine to $(\text{Mg,Fe})_2\text{SiO}_4$ β phase and of $(\text{Mg,Fe})_2\text{SiO}_4$ spinel to $(\text{Mg,Fe})\text{SiO}_3$ perovskite + $(\text{Mg,Fe})\text{O}$ magnesiowüstite. Recent seismic data suggest that these mantle discontinuities are thinner than predicted from the equilibrium phase diagrams for adiabatic geotherms (4). Solomatov and Stevenson (5) have recently argued that the sharpness of the 410-km and 660-km discontinuities may be a result of sluggish reaction kinetics and nonequilibrium phase transformations as material convects across the phase boundary. The key parameter in their kinetic model is the nucleation rate and, in particular, the depth (that is, pressure) to which an equilibrium

phase boundary can be overstepped before nucleation occurs. Similarly, in subduction zones, the depth to which olivine can be transported before it transforms into its more dense polymorphs is also controlled by reaction kinetics (6, 7). In this case, nucleation kinetics are especially important in relatively warm subduction zones and the warmer regions of cold subducting slabs (7). Nucleation can be the rate-controlling step during metamorphic reactions in the Earth's crust (8) and can result in the crystallization of nonequilibrium mineral assemblages (9).

Theoretically, nucleation kinetics are sensitive to both the strain energy and interfacial energy that accompany nucleation (5, 10, 11). Both of these parameters are poorly constrained for mineralogical reactions largely because of the limited number of experimental studies of nucleation kinetics (11, 12). For simplicity, nucleation during high-pressure polymorphic mineral transformations has generally been studied experimentally in single-phase polycrystalline aggregates (11–13). We demonstrate here, however, that in the case of the olivine-spinel transformation, the presence of

clinoenstatite has a strong effect on the kinetics of spinel nucleation.

We performed experiments at high pressure and temperature using a multianvil apparatus (14) with a starting material consisting of powdered San Carlos olivine ($\text{Mg}_{1.8}\text{Fe}_{0.2}\text{SiO}_4$) plus a few percent of Mg-rich orthopyroxene. Each experiment consisted of two stages: (i) hot pressing in the stability field of olivine + high clinoenstatite at 1523 K and 10 to 11 GPa for 2.5 to 3.0 hours and (ii) reaction to high-pressure phases at 1173 to 1273 K and 14 to 15 GPa for up to 12 hours. For the olivine component, these latter conditions lie in the stability field (Fig. 1) of either β phase or β phase + spinel (15). Between the hot-pressing and transformation stages, the temperature was reduced to 873 K to prevent transformation during the second compression.

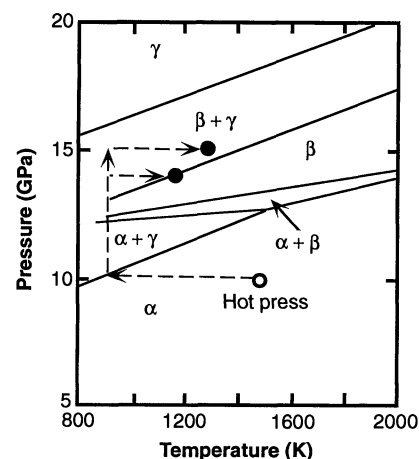


Fig. 1. Phase diagram for the $(\text{Mg}_{1.8}\text{Fe}_{0.2})_2\text{SiO}_4$ system (15) showing the experimental run conditions. The open circle represents the hot-pressing conditions and the solid circles show the transformation conditions. The arrows represent the paths followed from hot pressing to the transformation conditions. The stability fields are labeled as α (olivine), β (β phase), or γ (spinel).

Bayerisches Geoinstitut, Universität Bayreuth, D-95440 Bayreuth, Germany.

*To whom correspondence should be addressed.

Once at high pressure, the sample was heated at 100 K/min to the desired temperature.

The hot-pressing stage, which was necessary to produce an equilibrium microstructure in the starting material (16), resulted in an aggregate consisting of olivine grains 10 to 15 μm in diameter with a minor amount of small (0.5- to 5- μm diameter) grains of $(\text{Mg,Fe})\text{SiO}_3$ clinopyroxene (Fig. 2A). Hot-pressed samples have low densities of dislocations and other defects that form during pressurization of powdered samples; these defects can enhance reaction kinetics by acting as sites for heterogeneous nucleation.

The $(\text{Mg,Fe})\text{SiO}_3$ component was present in all hot-pressed and reacted samples as a Mg-rich $[\text{Mg}/(\text{Mg}+\text{Fe}) = 0.92]$ clinopyroxene, which we will refer to as clinoenstatite (Table 1). We infer that this phase formed during decompression by the inversion of high clinoenstatite (hcn), which is the stable but unquenchable $(\text{Mg,Fe})\text{SiO}_3$ polymorph under the conditions of hot pressing and reaction (17). The failure of the high clinoenstatite to transform to β phase + stishovite at 14 to 15 GPa (18) indicates either that the phase boundary was not overstepped or that the reaction was kinetically hindered (19).

In all of the samples reacted at high temperature (1173 to 1273 K) and pressure (14 to 15 GPa), small but varying amounts of olivine were transformed to either spinel or β phase (Table 1). In contrast, there was no detectable transformation in a sample that was pressurized to 14 GPa at 873 K and then quenched. In samples reacted for 0 to 1 hour at 1173 and 1273 K, we found small grains of spinel in contact with clinoenstatite at clinoenstatite-olivine grain boundaries (Fig. 2A). The zero-time and 1173 K experiments produced only spinel, indicating that the transformation began with the nucleation of spinel on clinoenstatite grains. In both of these samples, the spinel nucleated with a specific crystallographic orientation relation to clinoenstatite. Intermediate experimental durations produced the same spinel-clinoenstatite microstructure

(Fig. 2B) but with varying amounts of β phase immediately adjacent to clinoenstatite and spinel. In the longest duration experiment (12 hours), β phase is the predominant high-pressure phase (Fig. 2C), but small amounts of spinel still occur in contact with some pyroxene grains. In the samples that contain both spinel and β phase, we find coherent intergrowths of these two spineloid structures (Fig. 2D), which suggest that either the spinel transformed topotaxially to β phase or that the spinel provided a site for coherent nucleation of β phase. The transformation of olivine to either the spinel or β -phase structures under these reaction conditions occurred almost exclusively adjacent to high-clinoenstatite grains. Only one example of spinel + β phase without clinoenstatite was observed (Fig. 2D), but an adjacent pyroxene grain may have been present outside the plane of the sample foil.

The orientation relations that we observe between clinoenstatite and spinel and between β phase and spinel are the result of coherent nucleation. All observed pairs of spinel (γ) and clinoenstatite (cen) are crystallographically related such that $(100)_{\text{cen}}$ parallels $\{111\}_{\gamma}$ and $[010]_{\text{cen}}$ parallels $(110)_{\gamma}$ (Fig. 2B). This orientation relation, which is the same as that observed between orthopyroxene and hercynite spinel in a natural symplectite (20), results in the close-packed oxygen planes $[(100)_{\text{hcn}}$ and $\{111\}_{\gamma}]$ of the two structures being parallel and possibly continuous (Fig. 3A). The similarity between the high-clinoenstatite and spinel structures enables enstatite to act as a template for the coherent nucleation of spinel through the formation of a low-energy interface between the enstatite and the spinel nucleus. The crystallographic relation between spinel and β phase is the same as that previously reported (16, 21, 22) where $[010]_{\beta}$ parallels $\langle 110 \rangle_{\gamma}$ and the β -phase crystallographic axis c_{β} parallels $(100)_{\gamma}$.

Because the spinel structure fits well with both the high-clinoenstatite and the β -phase structures (Fig. 2, B and D), one might expect β phase to also form coherently on clinoenstatite. Combining the above orientation relations for the hcn-spinel and spinel- β phase intergrowths, we can determine a possible orientation relation for hcn- β phase: $(100)_{\text{hcn}}$ parallels $\{101\}_{\beta}$ and $[010]_{\text{hcn}}$ parallels $[010]_{\beta}$ (Fig. 3B). The misfit along the hcn (100) plane [also $(101)_{\beta}$ and $(111)_{\gamma}$] is small in both the hcn-spinel and hcn- β phase models (Fig. 3). It is also apparent that β phase has a slightly more distorted close-packed structure than either spinel or high clinoensta-

te.

Table 1. Experimental conditions and products. Minerals observed are olivine (ol), clinoenstatite (cen), spinel (γ), and β phase (β). Parentheses indicate minor occurrences.

Run	P (GPa)	T (K)	Time (hours)	Results
AB7	10	1473	2.45	ol + cen
AB6	14	873	0.00	ol + cen
AB5	14	1173	1.00	ol + cen + γ
AB12	15	1273	0.00	ol + cen + (γ)
AB9	15	1273	0.50	ol + cen + γ + (β)
AB8	15	1273	1.00	ol + cen + γ + β
AB10	15	1273	1.5	ol + cen + γ + β
AB11	15	1273	12.0	ol + β + cen + γ

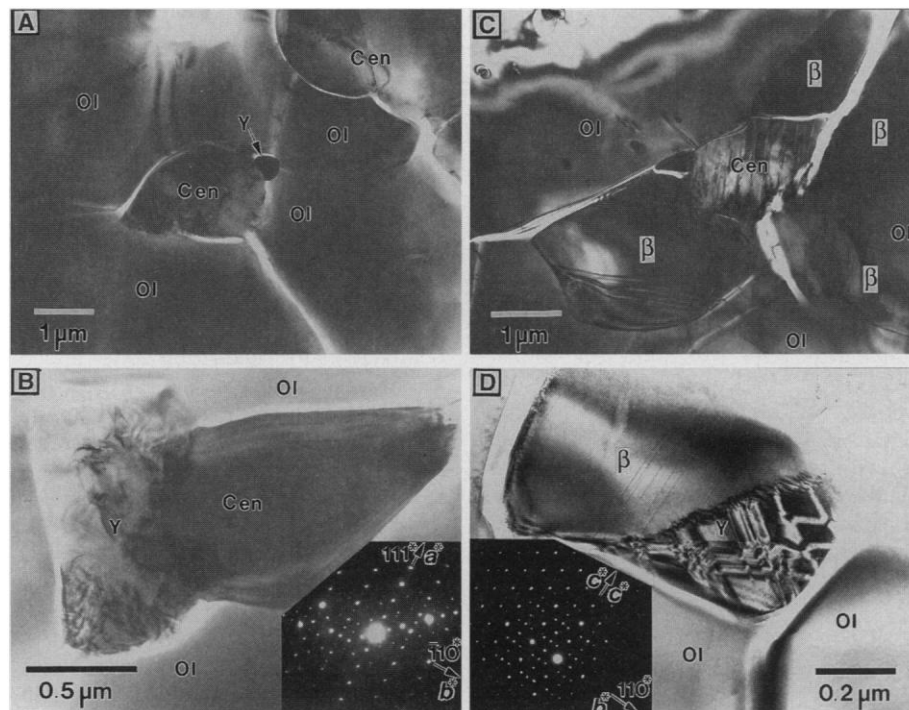


Fig. 2. Transmission electron micrographs showing the microstructural development with increasing time. Heating to 1273 K in the zero-time experiment (A) results in the nucleation of spinel (γ) on clinoenstatite (cen) grains at grain boundaries with olivine (ol). After 30 min at 1273 K and 15 GPa (B), clinoenstatite grains are capped by spinel. The selected area electron diffraction pattern (inset to B) shows the crystallographic relation: 111_{γ}^* parallels a_{cen}^* and 110_{γ}^* parallels b_{cen}^* . After 12 hours at 1273 K and 15 GPa (C), clinoenstatite grains are predominantly surrounded by β phase (β). In samples representing intermediate run durations, spinel and β phase are commonly intergrown (D) with the orientation relation c_{β}^* parallels $(100)_{\gamma}$ and b_{β}^* parallels $(110)_{\gamma}$.

tite, and therefore one would expect additional misfit strain energy in hcen- β phase intergrowths.

The actual misfit between high clinoenstatite and spinel or β phase at the pressure and temperature conditions of the runs was not calculated because of the paucity of

compressibility data at high temperature. Similarly, we did not compare misfits at atmospheric pressure because high clinoenstatite is not quenchable to 1 atm. We have therefore compared the structures at conditions (7.93 GPa, 300 K) for which data is available for high clinoenstatite (23). Cell

parameters for Mg_2SiO_4 β phase and spinel at these conditions were calculated from molar volume and compressibility data (24, 25). Misfit along the crystallographic directions given in the above orientation relations are small for both hcen- β phase and hcen-spinel intergrowths, with the largest misfit being normal to the close-packed oxygen planes (Table 2). The fit for the hcen-spinel intergrowth is somewhat better than for hcen- β phase, which may explain the preference for spinel over β -phase nucleation in our experiments.

The predominance of β phase in the longer duration experiments suggests that it is a stable phase at our experimental conditions. Because of the ease with which metastable spinel can form during the transformation of olivine to β phase (16, 22) and because of uncertainties in both the Mg_2SiO_4 - Fe_2SiO_4 phase diagram and the estimated pressures of the experiments, the experimental pressure and temperature conditions could lie either in the β phase + spinel or β -phase stability fields (Fig. 1). The compositions of the spinel grains [$\text{Mg}/(\text{Mg}+\text{Fe}) = 0.75$ to 0.80] are more Fe-rich than the β -phase grains [$\text{Mg}/(\text{Mg}+\text{Fe}) = 0.90$], which suggests nucleation within the β phase + spinel stability field. The predominance of β phase in the longer experiments is consistent with the proximity to the equilibrium phase boundary between β phase + spinel and β -phase stability fields (Fig. 1).

The ubiquitous association of spinel and β phase with clinoenstatite indicates that these product phases have only nucleated because of the presence of clinoenstatite. In previous studies of the olivine-spinel transformation, performed on polycrystalline olivine aggregates, the high-pressure polymorphs nucleated on olivine grain boundaries (16). The fact that this has not occurred in the present study indicates that the rate of nucleation of β phase and spinel on olivine grain boundaries is very low compared to the rate of spinel nucleation on olivine-clinoenstatite boundaries at the pressures and temperatures of our experiments. Therefore, clinoenstatite in an olivine aggregate acts as a catalyst by enhancing the kinetics of spinel nucleation and thereby also affects the overall transformation kinetics.

The microstructures observed here demonstrate that a second mineral phase, high clinoenstatite, can strongly influence the nucleation mechanisms and kinetics of olivine phase transformations. These results suggest that enstatite, the second-most-abundant phase in subducting lithosphere and upper mantle lithologies, is likely to enhance nucleation of spinel and possibly β phase within the Earth's mantle. Enhanced nucleation may have important effects on subduction, where sluggish reaction kinetics can result in a deeply subducted wedge of

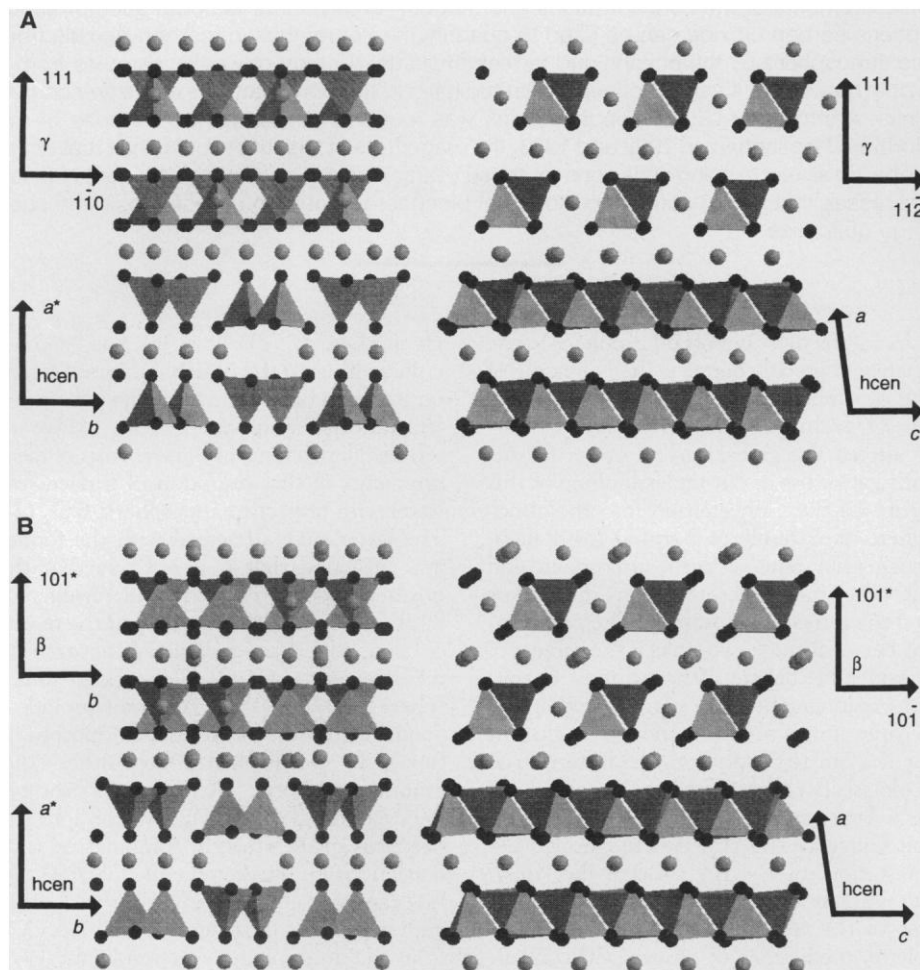


Fig. 3. Polyhedral representations of the crystal structures illustrating coherent intergrowths of (A) high clinoenstatite (hcn) with spinel (γ) and (B) high clinoenstatite with β phase. The structures are viewed along the [001] and [010] zone axes of high clinoenstatite, which correspond to the $\langle 112 \rangle$ and $\langle 110 \rangle$ of spinel and the [101] and [010] of β phase, respectively. The interfaces have been arbitrarily modeled parallel to the $(100)_{\text{hcn}}$ planes such that the Mg positions of the structures are superimposed in the projection and the close-packed stacking sequences of oxygens are preserved. Si positions are shown as tetrahedra with oxygens occupying the corners and Mg as the remaining atoms between oxygen layers.

Table 2. Orientation relations and misfit among spinel, high clinoenstatite, and β phase at 298 K and 7.93 GPa. Misfit is calculated as the difference in interplanar d spacings or vector lengths relative to spinel or β phase.

Orientation	γ -hcn		β -hcn		
	Planes, axes	Misfit Result (%)	Planes, axes	Misfit Result (%)	
$\{111\}_{\gamma} \parallel (100)_{\text{hcn}}$	$d_{111} - d_{200}$	2.45	$\{101\}_{\beta} \parallel (100)_{\text{hcn}}$	$d_{101} - d_{200}$	2.40
$\langle 110 \rangle_{\gamma} \parallel b_{\text{hcn}}$	$\frac{1}{2} \langle 110 \rangle - \frac{2}{3} b $	-1.52	$b_{\beta} \parallel b_{\text{hcn}}$	$\frac{1}{4} b - \frac{1}{3} b $	-1.91
$\langle 112 \rangle_{\gamma} \parallel c_{\text{hcn}}$	$\frac{3}{2} \langle 112 \rangle - c $	-0.12	$\langle 101 \rangle_{\beta} \parallel c_{\text{hcn}}$	$\frac{1}{2} \langle 101 \rangle - c $	0.52

metastable olivine (6, 7) and deep focus earthquakes through transformational faulting (26–28), and on mantle discontinuities (5), where nucleation kinetics can affect discontinuity thickness.

REFERENCES AND NOTES

1. D. L. Anderson, *Theory of the Earth* (Blackwell, Boston, 1989).
2. A. E. Ringwood, *Geochim. Cosmochim. Acta* **55**, 2083 (1991).
3. R. Jeanloz, *Geophys. Res. Lett.* **18**, 1743 (1991).
4. H. M. Benz and J. E. Vidale, *Nature* **365**, 147 (1993).
5. V. S. Solomatov and D. J. Stevenson, *Earth Planet. Sci. Lett.* **125**, 267 (1995).
6. C. M. Sung and R. G. Burns, *Tectonophysics* **31**, 1 (1976).
7. D. C. Rubie and C. R. Ross, *Phys. Earth Planet. Inter.* **86**, 223 (1994).
8. G. J. Wayte, R. H. Worden, D. C. Rubie, G. T. R. Droop, *Contrib. Mineral. Petrol.* **101**, 426 (1989).
9. D. C. Rubie, *Terra Abstr.* **7**, 113 (1995).
10. J. W. Christian, *The Theory of Phase Transformations in Metals and Alloys* (Pergamon, Oxford, 1965).
11. M. Liu and R. A. Yund, *Phys. Earth Planet. Inter.*, in press.
12. D. C. Rubie *et al.*, *J. Geophys. Res.* **95**, 15829 (1990).
13. B. R. Hacker, S. H. Kirby, S. R. Bohlen, *Science* **258**, 110 (1992).
14. The pressure medium for the experiments was a MgO octahedron with a 14-mm edge length, containing a stepped LaCrO₃ resistive heater [D. C. Rubie, S. Karato, H. Yan, H. St. C. O'Neill, *Phys. Chem. Miner.* **20**, 315 (1993)]. The assembly was compressed with Toshiba F-grade WC anvils with 8-mm truncations. The sample pressure was calibrated at 1473 K by reversing phase transitions in the SiO₂ and Mg₂SiO₄ systems, with a resulting uncertainty of approximately ±1 GPa. A contribution to the pressure uncertainty results from further pressurizing the sample at 873 K after hot pressing, a procedure that is different from the single-stage compression used for pressure calibration. Temperature was monitored with a W3%Re-W25%Re thermocouple without correction for the effect of pressure. The samples were loaded into 1.6-mm-diameter capsules and dried for several hours at 503 K in a vacuum oven before the experiments.
15. M. Akaogi, E. Ito, A. Navrotsky, *J. Geophys. Res.* **94**, 15663 (1989).
16. A. J. Brearley, D. C. Rubie, E. Ito, *Phys. Chem. Miner.* **18**, 343 (1992).
17. R. J. Angel, A. Chopelas, N. L. Ross, *Nature* **358**, 322 (1992). We refer to our Mg-rich clinopyroxenes as clinoenstatite in the quenched samples and as high clinoenstatite at transformation conditions.
18. R. Jeanloz and A. B. Thompson, *Rev. Geophys. Space Phys.* **21**, 51 (1983).
19. A. Hogrefe, D. C. Rubie, T. G. Sharp, F. Seifert, *Nature* **372**, 351 (1994).
20. Overprinted eclogite-grade rocks from the Bohemian Massif contain symplectites of orthopyroxene and hercynite spinel after garnet [P. J. O'Brien, *J. Metamorph. Geol.* **11**, 241 (1993)]. The orthopyroxene and spinel have the same crystallographic relation as that observed here (T. G. Sharp, unpublished results).
21. A. J. Brearley and D. C. Rubie, *Phys. Earth Planet. Inter.* **86**, 45 (1994).
22. D. C. Rubie and A. J. Brearley, *Nature* **348**, 628 (1990).
23. R. J. Angel and D. Hugh-Jones, *J. Geophys. Res.* **99**, 19777 (1994).
24. Y. Fei, S. K. Saxena, A. Navrotsky, *ibid.* **95**, 6915 (1990).
25. Y. Fei, H.-K. Mao, J. Shu, *ibid.* **97**, 4489 (1992).
26. S. H. Kirby, W. B. Durham, L. A. Stern, *Science* **252**, 216 (1991).
27. P. C. Burnley, H. W. Green, D. J. Prior, *J. Geophys. Res.* **96**, 425 (1991).
28. H. W. Green and P. C. Burnley, *Nature* **341**, 733 (1989).

8 February 1995; accepted 19 May 1995

A Large Northern Hemisphere Terrestrial CO₂ Sink Indicated by the ¹³C/¹²C Ratio of Atmospheric CO₂

P. Ciais, P. P. Tans, M. Trolrier, J. W. C. White,* R. J. Francey

Measurements of the concentrations and carbon-13/carbon-12 isotope ratios of atmospheric carbon dioxide can be used to quantify the net removal of carbon dioxide from the atmosphere by the oceans and terrestrial plants. A study of weekly samples from a global network of 43 sites defined the latitudinal and temporal patterns of the two carbon sinks. A strong terrestrial biospheric sink was found in the temperate latitudes of the Northern Hemisphere in 1992 and 1993, the magnitude of which is roughly half that of the global fossil fuel burning emissions for those years. The challenge now is to identify those processes that would cause the terrestrial biosphere to absorb carbon dioxide in such large quantities.

One of the most important problems in the science of global change is the balancing of the global budget for atmospheric CO₂. Although anthropogenic activities have clearly altered the global carbon cycle, significant gaps exist in our understanding of this cycle. Of the CO₂ emitted into the atmosphere as a result of burning fossil fuels, roughly half remains in the atmosphere and the other half is absorbed into the oceans and the terrestrial biosphere. The partitioning between these two sinks is the subject of considerable debate. Whereas most chemical oceanographers are confident that the oceanic sink is not large enough to account for the entire absorption, many terrestrial ecologists doubt that the land biosphere can be a large carbon sink, particularly given the source to the atmosphere through deforestation, hence, the issue of the "missing" carbon sink. Without a good accounting for the fate of CO₂ leaving the atmosphere, predictions of future CO₂ concentrations that result from different emission scenarios will remain uncertain. This, in turn, weakens the link between energy policy and climate change.

Observations of the north-south gradient of atmospheric CO₂ show that there must be a large carbon sink in the Northern

Hemisphere (1, 2). This sink has been ascribed either to the North Atlantic Ocean, on the basis of sparse measurements of ¹³C/¹²C ratios in atmospheric CO₂ (1), or to terrestrial mechanisms, on the basis of measurements of the saturation of surface seawater with respect to atmospheric CO₂ (2). The latter study disagreed with the former and suggested that it is unlikely that the northern oceans could be responsible for most of the sink. Here we present the results of a greatly expanded global network of measurements of ¹³C/¹²C ratios in atmospheric CO₂. The ¹³C/¹²C ratios provide a good fingerprint of terrestrial biospheric fluxes of CO₂, as plant photosynthesis discriminates against ¹³C, whereas isotopic fractionation during CO₂ invasion into the oceans is small. Thus, in combination with concentration measurements, ¹³C/¹²C ratios can be used to distinguish the oceanic and terrestrial biospheric fluxes of CO₂ from the atmosphere. Our results for 1992 and 1993 indicate that a strong terrestrial biospheric carbon sink existed in the temperate latitudes of the Northern Hemisphere during those years with a magnitude roughly half that of the global fossil fuel burning flux.

Since 1990, the Stable Isotope Laboratory at the Institute of Arctic and Alpine Research (INSTAAR) has measured δ¹³C (3) in CO₂ from weekly samples of air from a network of sites, complementing measurements of CO₂ mixing ratios made by the National Oceanic and Atmospheric Administration's Climate Monitoring and Diagnostics Laboratory (NOAA/CMDL). In 1992 and 1993, 41 sites from this network were measured for δ¹³C. These data were augmented by measurements made by the Commonwealth Scientific and Industrial Research Organisation (CSIRO) from two sites (4) at high southern latitudes (Fig. 1). From the smoothed atmospheric observations, the latitudinal distribution of the sur-

P. Ciais, National Oceanic and Atmospheric Administration's Climate Monitoring and Diagnostics Laboratory (NOAA/CMDL), R/E/CG1, 325 Broadway, Boulder, CO 80303, USA, and LMCE-DSM Commissariat a l'Energie Atomique, L'Orme des Meurisiens, 91191, Gif sur Yvette Cedex, France.

P. P. Tans, NOAA/CMDL, R/E/CG1, 325 Broadway, Boulder, CO 80303, USA.

M. Trolrier, NOAA/CMDL, R/E/CG1, 325 Broadway, Boulder, CO 80303, USA, and Institute of Arctic and Alpine Research (INSTAAR), University of Colorado, Boulder, CO 80309, USA.

J. W. C. White, INSTAAR, and Department of Geological Sciences, University of Colorado, Boulder, CO 80309, USA.

R. J. Francey, Commonwealth Scientific and Industrial Research Organisation, Division of Atmospheric Research, Mordialloc, Victoria 3195, Australia.

*To whom correspondence should be addressed.